Wireless potentiometry of thermochemical heterogeneous catalysis

Neil K. Razdan, Karl S. Westendorff, Yogesh Surendranath*

Department of Chemistry, Massachusetts Institute of Technology, Cambridge, Massachusetts 02139, United States

Abstract: Catalyst surfaces in contact with liquid media are subject to spontaneous charge transfer reactions that electrically polarize the solid-liquid interface. Consequently, the electrochemical potential, E_{cat}, of the surface is a critical parameter that defines the free-energy landscape of catalysis. E_{cat} can be readily measured for a catalyst supported on a conductive material and wired to an external circuit but is difficult to quantify for the vast majority of thermochemical catalysts that are supported on electrical insulators. This measurement gap has impeded a unifying understanding of the role of electrochemical polarization in thermochemical catalysis. Herein, we develop a methodology for quantifying E_{cat} of metal catalysts supported on insulators by introducing a small concentration of a redox-active molecule to establish a wireless electrical connection between the dispersed catalyst and an inert sensing electrode. We validate this approach by quantifying E_{cat} during catalytic reactions involving H_2 or O_2 in water and acetonitrile solvent. Using this methodology, we expose distinct rate-potential scalings for aerobic formic acid oxidation catalysis on SiO_2- and Al_2O_3- versus TiO_2-supported Pt catalysts. The methodology we develop herein enables the broad-based investigation of the role of electrochemical polarization in thermochemical catalysis.

Interfacial polarization is a key determinant of reactivity in solid-liquid heterogeneous catalysis[1–8]. Even in the absence of external bias, solid catalysts immersed in liquid media spontaneously polarize due to differences in the (electro-)chemical potential between the two phases. These energetic differences are resolved by the movement of both charged and uncharged liquid-phase species, resulting in the formation of a highly polarized interfacial region known as the electrical double layer (EDL)[9]. The EDL arises at *all* solid-liquid interfaces and, in the case of a supported metal catalyst (e.g., Pt/SiO_2), furnishes electrically-conductive domains of the solid material (e.g., Pt nanoparticles) with a well-defined electrochemical potential, E_{cat}. The catalyst open-circuit potential, E_{cat}, is, thus, a salient descriptor of interfacial polarization during heterogeneous catalysis and provides a wealth of information that reflects adsorbate speciation[10,11], extents of catalyst deactivation[12–14], interfacial concentration gradients[6,11,15], and more[7,16]. Measurement of E_{cat} is therefore a (i) prerequisite to any investigation of polarization-influenced reactivity and (ii) highly enabling for detailed mechanistic analyses, functional characterization, and rational design of new catalysts. For example, monitoring E_{cat} during (de-)hydrogenation and aerobic oxidation reactions has been shown to report on O_2 mass transport limitations[6,11], rate-determining step identity[13], and mechanisms of cooperativity between metal active sites[17,18]. However, these studies have, with few exceptions[7,19], been limited to use of electrode-supported catalysts (**Figure 1A**)[6,8,11,13,17,18,20,21] formulated primarily by a small community of researchers specialized in the intersection of thermochemical and electrochemical catalysis. This approach is dissonant with the majority of reactor designs for solid-liquid heterogeneous catalysis that use solution-dispersed powder catalysts commonly comprised of metal nanoparticles supported on electronically insulating oxides (e.g., SiO_2, Al_2O_3, TiO_2). These distributed, poorly conductive materials cannot be connected to macroscopic wires for E_{cat} detection (**Figure 1B**). This incompatibility represents a fundamental impasse to the measurement of E_{cat}—and therefore the understanding of underpinning electrochemical phenomena—in heterogeneous catalysis research.

In this work, we develop a generalizable, non-intrusive methodology for quantifying E_{cat} for dispersed catalysts supported on insulators. Specifically, we show that the introduction of small concentrations (~100 μM) of redox-active molecules serves to establish a wireless electrical connection between dispersed catalyst particles and an inert sensing electrode (**Figure 1C**). This approach is conceptually related to but distinct from molecule-mediated heterogeneous (electro-)catalysis. Mediated catalysis employs redox-active molecules as kinetically-relevant proton/electron shuttles to tune E_{cat} and/or steer catalytic redox events[5,22–27]. In contrast, the methodology in this work uses redox-active molecules as dilute, catalytically non-invasive sensing agents that detect native E_{cat} without altering catalytic function. Using the interconversion of H_2 and H^+ as a model reaction for pinning the catalyst potential, we validate the accuracy and rapid response time of wireless potentiometry for SiO_2, Al_2O_3, TiO_2 support Pt nanoparticles across an E_{cat} span of ~840 mV in water or acetonitrile solvent and across a H^+ activity range of ≥12 pH units. Employing the insights from these validation studies, we rationally design a system for operando quantification of E_{cat} during aqueous aerobic oxidation of formic acid. Quantification of E_{cat}

during reaction between HCOOH and O_2 reveals underlying differences in catalytic function between supported Pt materials that are obscured by thermochemical analyses alone. Despite exhibiting near identical HCOOH reaction orders, SiO_2-, TiO_2-, and Al_2O_3-supported catalysts polarize to potentials that vary by as much as ~60 mV—the equivalent of 5.8 kJ mol^{-1} in energetic driving force. Correspondingly, the scaling between reaction rate and catalyst potential varies by 2.3× (127 – 289 mV dec^{-1}), indicating that these catalysts respond to interfacial polarization in substantially different ways. These findings demonstrate that (i) measurement of E_{cat} is an enabling tool that can provide catalytic information complementary to conventional thermochemical measurements of rate/selectivity and (ii) even electronically insulating supports can play a key role in determining the potential sensitivity of metal-catalyzed reactions.

RESULTS AND DISCUSSION

Design considerations for wireless potentiometry of heterogeneous catalysts

The wireless potential sensing method developed herein uses redox-active molecules in lieu of macroscopic wires to convey electrons between solution-dispersed catalyst particles and a sensing electrode—as shown in **Figure 1C**. We envision that reduced (*Red*) and oxidized (Ox^+) forms of the molecular redox couple will engage in outer-sphere electron transfer (OSET) with catalyst particles to equilibrate the solution and catalyst potentials. Realizing this scheme requires careful selection of the redox pair to satisfy the following criteria:

(1) *The redox couple must display facile electron transfer kinetics at potentials in the vicinity of* E_{cat}.

In effect, this criterion amounts to requiring that the difference between E_{cat} and the equilibrium potential of the *Red*/Ox^+ redox couple, E^0_{Red/Ox^+}, is not too large ($\lesssim$ 180 mV). This can be seen by examination of the Nernst equation describing equilibration of electrochemical potentials of the catalyst particles and the *Red*/Ox^+ couple

$$E_{cat} = E_{probe} = E^0_{Red/Ox^+} + \frac{RT}{nF}\ln\frac{a_{Red}}{a_{Ox}} \qquad \textbf{Equation 1}$$

where a_i is the thermodynamic activity of species i, R is the gas constant, T is temperature, and $E^0_{Red/Ox}$ and n are respectively the equilibrium potential and electron stoichiometry of the *Red*/Ox^+ redox couple. From examination of **Equation 1**, we see that increasing differences between E_{cat} and E^0_{Red/Ox^+} engender increasingly large ratios between *Red* and Ox^+ activities. If the difference between E_{cat} and E^0_{Red/Ox^+} is too large, the corresponding equilibrium ratio of *Red* and Ox^+ may be unachievable due to attenuated OSET kinetics for the minority redox state. Therefore, as a heuristic, we suggest the *Red*-to-Ox^+ ratio should not exceed ~1000×, corresponding to $\left|E_{cat} - E^0_{Red/Ox^+}\right| < 180$ mV. However, we do not exclude the possibility that potential sensing may be efficacious even beyond >180 mV deviations between E^0_{Red/Ox^+} and E_{cat} if *Red*/Ox^+ redox kinetics are particularly facile.

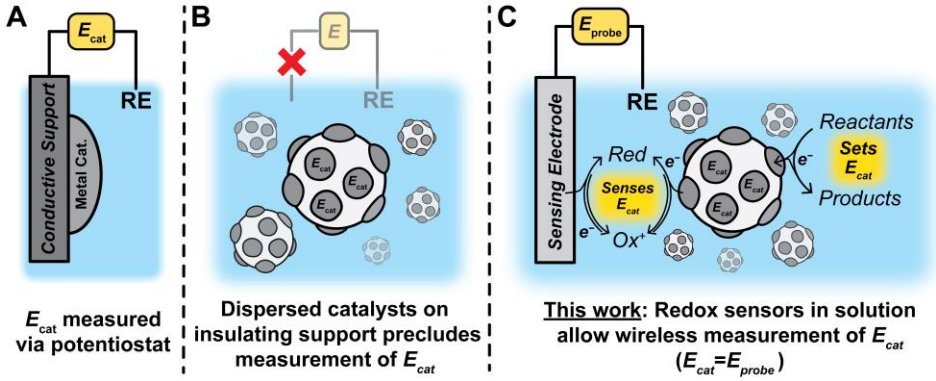

Figure 1 | Wired and wireless electrochemical potential measurement. Conventionally, **(A)** electrode-supported metal catalysts can be directly connected to an external circuit, enabling facile E_{cat} measurement. In contrast, **(B)** metal catalysts supported on insulating materials (e.g., SiO_2) cannot be readily interfaced with macroscopic wires. In this work, **(C)** the electrochemical potential of dispersed, supported metal catalysts, E_{cat}, is detected by monitoring the open-circuit potential of a sensing probe electrode, E_{probe}. Equilibration of E_{cat} and E_{probe} is mediated by outer-sphere electron transfer of the catalyst and probe electrode to/from a dilute molecular redox pair (*Red*/Ox^+).

(2) *The redox couple must be present in dilute concentrations.*

In principle, OSET between the catalyst and *Red*/Ox^+ couple could indirectly perturb catalytic function by causing a variation in E_{cat} correspondent to the flow of electrons to Ox^+ or from *Red*. In fact, such phenomena have been leveraged to intentionally specify E_{cat} of dispersed catalysts by addition of high concentrations (~10 mM) of *Red* and Ox^+ in appropriate ratios[5,26,28]. To sense E_{cat} without perturbation, we use dilute concentrations (~10 μM) of redox active molecules to ensure that the net flow of electrons to Ox^+ or from *Red* is sufficiently small as to minimally perturb E_{cat}.

(3) *The redox couple must not perturb catalytic function.*

The redox pair must not interfere with catalysis by interacting with reactants, intermediates, or products. Fortunately, the envisaged mechanism of potential measurement is expected to fulfill this criterion in most cases. Specifically, to the extent that Ox^+ and *Red* engage purely in OSET with the catalyst particles, these species are expected to exchange electrons via tunneling, obviating the need to enter the EDL or adsorb the catalyst surface. Maximizing the outer-sphere character of ET to Ox^+ and *Red* should thus minimize site-blocking or interactions with surface intermediates. Nevertheless, the catalytic non-invasiveness of redox sensors must be evaluated on a case-by-case basis, as we detail below.

Provided that the above criteria are met, the proposed scheme in **Figure 1C** and **Equation 1** constitutes an authentic wireless electrical connection between dispersed catalysts and the probe electrode that minimizes the likelihood of interference with catalysis and is agnostic to both probe and catalyst identity. In the following, we validate the described mechanism of E_{cat} measurement by employing a model reaction that pins E_{cat} to a well-defined potential that is known *a priori*.

Validation of catalyst potential measurement through molecule-mediated redox sensing

We devise a model system to illustrate the proposed methodology by leveraging the reversibility of Pt-catalyzed interconversion of H_2 and solution-phase H^+

$$H^+ + e^- \rightleftharpoons \tfrac{1}{2} H_2 \qquad \textbf{Equation 2}$$

In both aqueous and non-aqueous media, the forward and reverse rates of H_2/H^+ catalysis on Pt equalize[15,29–31], establishing thermodynamic equilibrium as described by the Nernst equation

$$E_{\mathrm{RHE}} = E_{\mathrm{SHE}} - 0.058\ \mathrm{pH} - 0.029 \log_{10} P_{\mathrm{H_2}} \qquad \textbf{Equation 3}$$

where P_{H_2} is the partial pressure of H_2 in units of bar and E_{RHE} and E_{SHE} are the reversible hydrogen electrode (RHE) and standard hydrogen electrode (SHE) equilibrium potentials in units of volts. Equilibrium H_2/H^+ catalysis eliminates any uncertainty in E_{cat}, which is quantified by monitoring the potential of an *in situ* RHE reference electrode (see **Figure 2**). With E_{cat} spontaneously pinned to E_{RHE}, we examine the proposed wireless potential sensing approach by comparing the potential of a glassy carbon (GC) probe electrode, E_{probe}, to E_{RHE} using a silicotungstate redox sensor ($[SiW_{12}O_{40}]^{4-}$ or STA) as illustrated in **Figure 2**. STA is sequentially reducible through two one-electron OSET reactions that respectively occur with pH-independent equilibrium potentials of −187 mV and −445 mV relative to SHE[32]. The first of these redox features is 129 mV negative of the H_2/H^+ equilibrium potential in pH 1 electrolyte. Since this potential difference is within the 180-mV heuristic set forward above, we anticipate that the $[SiW_{12}O_{40}]^{4-}/[SiW_{12}O_{40}]^{5-}$ redox pair will equilibrate with H_2/H^+ catalysis and enable wireless potential sensing.

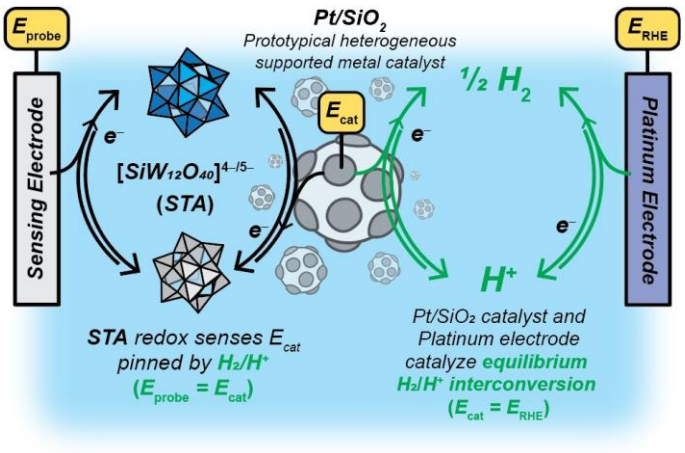

Figure 2 | Wireless potentiometry model system. Equilibrium H_2/H^+ catalysis affixes the potential of dispersed Pt/SiO_2 particles (E_{cat}) and an *in situ* Pt reversible hydrogen electrode (E_{RHE}). In turn, the equilibration of E_{cat} to E_{RHE} establishes the redox speciation of dilute silicotungstate anions that rapidly exchange electrons with the Pt/SiO_2. Silicotungstate anions then engage in outer sphere electron transfer with a glassy carbon sensing electrode, resulting in electronic equilibration throughout the system ($E_{probe} = E_{cat} = E_{RHE}$).

We evaluate this hypothesis by monitoring open-circuit potential transients of GC probe electrodes following the introduction of 1 bar H_2 to N_2-saturated, well-stirred 0.1 M $HClO_4$ electrolytes containing dispersed Pt/SiO_2 powders, shown in **Figure 3**. The data evince that, in the absence of STA, the potential of the GC electrode is largely unperturbed by the copresence of H_2, H^+, and Pt/SiO_2 catalyst. Indeed, after 300 seconds, E_{probe} remains >500 mV positive of E_{cat}. These results indicate that charge transfer events occurring during collisional contact between catalyst powders and GC probe electrode is an unreliable method to equilibrate E_{probe} with E_{cat}. We note, however, that with sufficiently vigorous magnetic stirring (≳2000 rpm) and large quantities of catalyst (≳3 g/L) GC electrodes can electronically equilibrate with supported Pt powders (Figure S1), consistent with prior observations.[33]

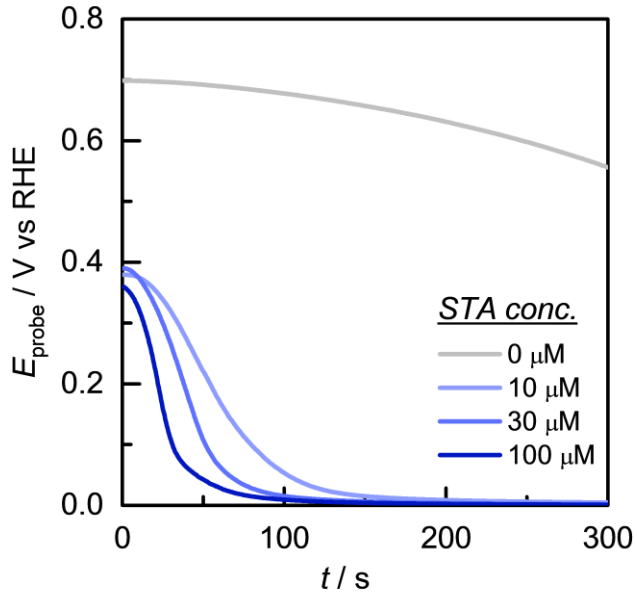

Figure 3 | Measurement of catalyst potential. The open-circuit potential of a GC electrode upon introduction of 1 bar H_2 to an N_2-saturated, stirred (1150 rpm) solution with 0.1 M $HClO_4$, 0.3 g/L of Pt/SiO_2 powder, and 0, 10, 30, or 100 μM STA. See Figure S2 and SI methods section for detailed cell design and experimental protocol.

The sensitivity of E_{probe} to H_2 introduction is improved by addition of 10, 30, or 100 μM $[SiW_{12}O_{40}]^{4-}$ (**Figure 3**, blue lines), resulting in equality of E_{probe} and E_{cat} within ~100 seconds. The data indicate that STA provides a conduit for charge

transfer between Pt/SiO_2 and the GC electrode that becomes increasingly facile with increasing concentration of STA. We therefore interpret the data in **Figure 3** to reflect a potential sensing mechanism mediated by reversible one-electron reduction of $[SiW_{12}O_{40}]^{4-}$ to $[SiW_{12}O_{40}]^{5-}$ by dispersed Pt/SiO_2 particles in accord with **Figure 2** and **Equation 1**. This mechanism of potential measurement is not unique to STA and extends to any redox agent that satisfies the design considerations outlined above. Similar potential sensing transients are observed with use of phosphotungstate anions, PTA (Figure S3), an analog of STA with redox features ~150 mV positive relative to the corresponding transitions in STA[32]. In the following, we further validate molecule-mediated potential measurement by evaluating the time-resolution of E_{probe} response to changes in H_2 partial pressure and pH.

Tracking dynamic changes in E_{cat} during catalytic transients

Time-resolved measurement of E_{cat} has the potential to facilitate mechanistic and kinetic analysis during catalytic transients (e.g., catalyst deactivation, or response to step-change in reactant concentration)[13,34–36]. However, the fidelity of this approach requires that the timescale of potential sensing is commensurate with the timescale of catalysis to ensure that $E_{probe} = E_{cat}$ at all times. To examine the timescale of potential sensing, we initiated step changes in H_2 or H^+ activity and tracked the temporal variation of the potential of an *in situ* Pt RHE electrode relative to the potential of an inert carbon probe electrode, E_{probe}. Based on the aforementioned heuristic (i.e., $|E_{RHE} - E^0_{Red/Ox}| < 180$ mV) and the equilibrium reduction potentials of STA (−187 mV and −445 mV *vs* SHE), we anticipate that STA is capable of sensing $E_{cat} = E_{RHE}$ for chemical activities corresponding to 0.1 – 10 bar H_2 and pH 0 – 5—providing wide H_2 pressure and H^+ activity windows within which to assess the dynamic responsiveness of E_{probe}.

We monitored the temporal evolution of GC and Pt electrode potentials upon variation in H_2 pressure, as shown in **Figure 4A** for electrolyte conditions identical to the case of 100 μM STA in **Figure 3**. From 0 to 1.5 ks, the H_2 pressure is constant at 0.5 bar and, correspondingly, the potential of the GC electrode (E_{probe}) and platinum electrode (E_{Pt}) are within ~2 mV. At 1.5 ks, the H_2 pressure is decreased to 0.1 bar (balanced by N_2) without altering the total flow rate (0.83 $cm^3\ s^{-1}$). Open-circuit potentials of both electrodes respond within seconds and equalize to a potential in accord with **Equation 3**. Similar responses to H_2 partial pressure are observed for subsequent steps to 0.2 bar and 1 bar. In each case, potential transients for GC and Pt electrodes are similar and stabilize to the predicted equilibrium potential, as is shown in Figure S4. The observation of nearly identical potential transients for E_{probe} and E_{Pt} in **Figure 4A** indicates that wireless potentiometry authentically quantifies native transients in E_{cat} without convolution from STA electron transfer or transport.

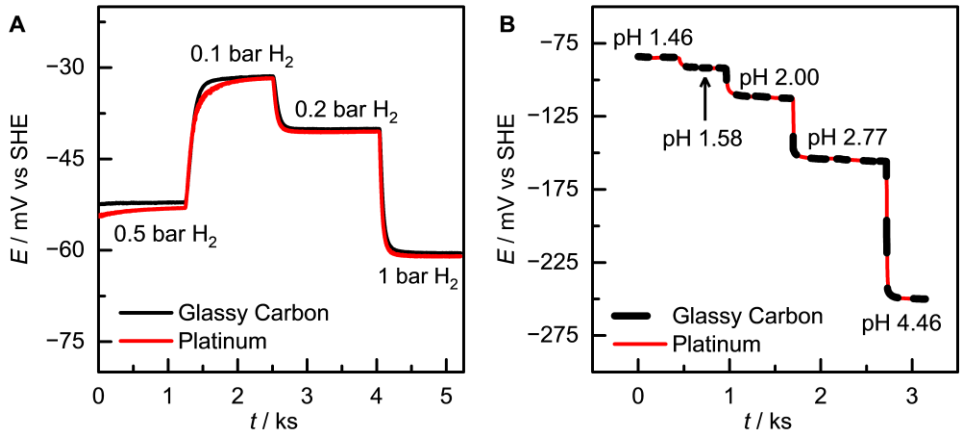

Figure 4 | Tracking transients in catalyst potential. Transients in the open-circuit potential of a glassy carbon (black) and platinum (red) electrode upon variation in **A)** H_2 partial pressure and **B)** pH in stirred solutions with 0.3 g/L of Pt/SiO_2 powder and 100 μM STA. See SI for detailed cell design and experimental protocol.

To further examine the fidelity of the methodology, we compare transients in E_{probe} and E_{Pt} upon changes in solution H^+ activity, or pH. **Figure 4B** shows the potential response of GC and Pt electrodes upon variation of pH by addition of 1 M NaOH to H_2-saturated, stirred aqueous solution containing 0.1 M Britton-Robinson buffer, 100 μM STA, and 0.3 g/L Pt/SiO_2. Changes to solution pH caused by NaOH addition are continuously measured by an *in situ* gas-tight pH sensor (Figure S4, Figure S5). Prior to the introduction of NaOH, the solution pH is 1.46 and the Pt and GC electrode potentials are stable and equivalent. Upon each addition of 1 M NaOH (indicated by potential drops in **Figure 4B**), the pH probe, Pt electrode, and GC electrode respond at comparable timescales, achieving stable pH or potential values within 10 – 100 seconds. Akin to **Figure 4A**, the similarity in temporal response between E_{probe} and E_{Pt} in **Figure 4B** suggests that STA redox reactions and mass transport are rapid on the timescale of these pH changes and that the transient in E_{probe} values are limited by the

timescale of changes in E_{cat} itself. Taken together, the responsiveness of E_{probe} to H_2 partial pressure (**Figure 4A**) and solution pH (**Figure 4B**) indicate that STA redox reactions are sufficiently facile to enable real time E_{cat} quantification in a fashion conducive to mechanistic and kinetic analysis.

Assessing generality of wireless potentiometry across reaction media

The foregoing potential sensing approach is, in principle, generalizable to any reaction medium provided appropriate choice of the redox sensor. In particular, we expect that E_{cat} during H_2/H^+ catalysis is readily detectable in both aqueous and organic solvents across wide ranges of H^+ activity. To test these hypotheses, we first extend the scope of redox sensing molecules beyond heteropolyanions such as PTA and STA[37], for potential sensing in aqueous media. Guided by the design principles set forth above, we selected methyl viologen (MV) and 2,5-dihydroxy-1,4-benzoquinone (DHBQ) as sensing molecules for pH 6.8, 12 and pH 14, respectively. MV is a bipyridinium dication that undergoes two facile one-electron reductions (E = −0.45 V and −0.88 V vs SHE) at potentials commensurate with E_{RHE} in its range of pH stability (~4 to ~12)[38–41]. DHBQ is a dihydroxybenzoquinone isomer that fully deprotonates in alkaline media to form a dianion that is reversibly reducible in an ostensibly concerted two-electron OSET event with E = 0.72 V vs SHE, a potential aligned with E_{RHE} for pH = 12 – 14. Based on these properties, we assess the H_2/H^+ potential sensing capabilities of MV and DHBQ in Britton Robinson buffers (pH = 6.8, 12) and 1 M KOH (pH = 14) respectively. In the case of MV, a Ti wire is used as a sensing electrode instead of glassy carbon. We find that use of GC with MV results in decelerated approach of E_{probe} to E_{RHE}, presumably due to the known propensity of reduced MV radical cations to agglomerate on carbon electrodes (Figure S7)[42].

We assess the potential sensing capabilities of DHBQ and MV by monitoring the potential response of GC button or Ti wire upon introduction of 1 bar H_2 to N_2-saturated electrolytes containing 0.15 g/L Pt/SiO_2 with or without 100 µM DHBQ or MV (**Figure 5**). In contrast to the sluggish or negligible response of E_{probe} upon introduction of H_2 in the absence of redox sensor (**Figure 5A & 5B**, grey), E_{probe} reaches E_{RHE} within ~100 s in the presence of the redox sensor for both conditions (**Figure 5A**, red **& Figure 5B**, blue). In the case of MV, approach of E_{probe} to E_{RHE} is also visually indicated by the appearance of a blue (**Figure 5B**; pH 6.8) or violet (Figure S8; pH 12) color correspondent to known optical properties of reduced viologens[38]. These findings are analogous to those in **Figure 3** for STA-mediated sensing of E_{cat} in 0.1 M $HClO_4$ with comparable concentrations of STA and Pt/SiO_2. For MV, the H_2/H^+ equilibrium potential is effectively sensed over range of MV concentrations spanning 10 µM to 1 mM (Figure S8). For DHBQ, H_2/H^+ equilibrium potential is well sensed for redox sensor concentrations ranging from 10 to 100 µM, but increasing the concentration to 1 mM impedes detection of the H_2/H^+ equilibrium potential (Figure S9), suggesting that higher DHBQ concentrations lead to (i) interference with Pt-mediated H_2/H^+ catalysis[22] or, possibly, (ii) parasitic dimerization of the reduced, diradical (dihydroxy)-semi-quinone[43]. These findings emphasize that the dependence of E_{probe} on sensor concentration should be assessed on a case-by-case basis for a given catalyst or reaction conditions to ensure against any convolution in the measured value of E_{cat}. Notwithstanding, the data in **Figure 3-5** and Figure S8 demonstrate the generalizability of wireless potential sensing across pH environments and molecular sensing agents in aqueous solutions (**Figure 5C**).

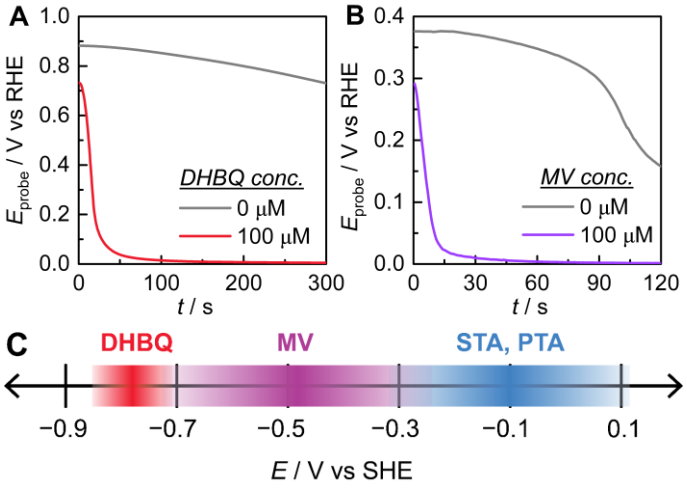

Figure 5 | Potential measurement in neutral and alkaline water. The open-circuit potential of a sensing electrode (**A)** GC, **B)** Ti) upon introduction of 1 bar H_2 to N_2-saturated, stirred (1150 rpm) solutions containing 0.15 g/L of Pt/SiO_2 and: **A)** 1 M KOH (pH 14) with or without 100 µM 2,5-dihydroxy-1,4-benzoquinone (DHBQ); or **B)** Britton Robinson buffer (pH 6.8) with or without 100 µM methyl viologen (MV). See SI for detailed cell design and experimental protocol. **C)** Span of H_2/H^+ potential sensing in aqueous media using STA, PTA, MV, and DHBQ. The depicted potential range for each sensing agent is determined by pH stability and molecular redox potentials (±180 mV).

Wireless potential sensing in acetonitrile (MeCN) follows the same conceptual principles as in aqueous systems, with H_2/H^+ catalysis used as a model reaction to specify $E_{cat} = E_{RHE}$. Prior studies establish that Pt electrodes in MeCN-based electrolytes catalyze reversible H_2/H^+ interconversion.[31] Consequently, the electrode open-circuit potential scales in a Nernstian fashion with proton donor pK_a and/or acid-to-base ratio of donor (HA)/acceptor(A^-) pairs in accordance with **Equation 4**:

$$E_{RHE}^{MeCN} = E_{SHE}^{MeCN} - 0.058\,\mathrm{pK_a} + 0.058\log_{10}\frac{a_{HA}}{a_{A^-}} \qquad \textbf{Equation 4}$$

where E_{RHE}^{MeCN} and $E_{SHE}^{MeCN} = -0.028$ V vs $E_{Fc/Fc+}^{MeCN}$ are respectively the pH-dependent and standard equilibrium potentials of H_2/H^+ redox in acetonitrile. In this work, we tune solution pH in acetonitrile by preparing one-to-one ratios of HA/A^- pairs with donor pK_a values ranging between 6.1 and 23.5[44,45]. Importantly, the acid-base pair and the redox sensor pair must be chemically compatible and so it best to employ weakly nucleophilic acid-base pairs and/or substitutionally inert transition metal complexes. In all cases, we recommend that the compatibility of redox sensor and acid/base pair be assessed independently (**Figure 6**; Figures S10-S15). In addition to mutual stability, pairing of sensor and buffer need also ensure that $E_{Red/Ox}^{0}$ is within ~180 mV of E_{RHE}^{MeCN} determined by buffer pK_a as per **Equation 4**.

With foregoing considerations in mind, we identified four sensor-buffer pairs that effectively detect equilibrium potentials of H_2/H^+ catalysis in MeCN media (**Figure 6**; Figures S10-S12). Examples of incompatible sensor-buffer pairs are provided in Figures S13-S15. Adapting the experimental cell setup describe above for aqueous media (**Figure 2**) to MeCN, we monitor the potential of a GC sensing electrodes, E_{probe}, during introduction of 1 bar H_2 to acetonitrile solutions containing 0.3 g/L Pt/SiO_2 and 10 mM HA/A^- buffer (see SI for details for buffer preparation) with and without 100 µM redox sensor. Given the wide variety of catalytic transformations that involve H_2O and/or O_2, we intentionally selected water- and air-stable redox sensors, ruthenium (III) acetylacetonate, $Ru(acac)_3$, decamethylferrocene, $Me_{10}Fc$, and octamethylferrocene, Me_8Fc.

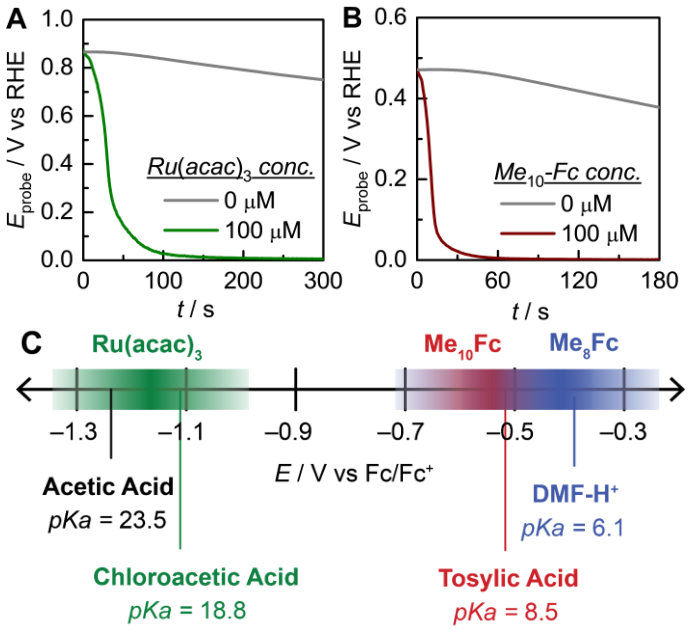

Figure 6 | Potential measurement in acetonitrile. The open-circuit potential of a GC electrode upon introduction of 1 bar H_2 to N_2-saturated, stirred (1150 rpm) solutions containing 0.1 M $TBAPF_6$, 0.5 g/L of Pt/SiO_2, and: **A)** 20 mM chloroacetic acid + 10 mM TBAOH●$30H_2O$ with or without 100 µM $Ru(acac)_3$; or **B)** 20 mM tosylic acid + 10 mM TBAOH●$30H_2O$ with or without 100 µM decamethylferrocene (Me_{10}-Fc). See SI for detailed cell design and experimental protocol. **C)** Span of H_2/H^+ potential sensing in acetonitrile media using $Ru(acac)_3$, Me_{10}-Fc, and Me_8-Fc. The depicted potential range for each sensing agent is ±180 mV of molecular redox potentials.

For both chloroacetic acid and tosylic acid buffers, the potential of GC probe electrodes (**Figure 6**, grey lines) responds slowly to H_2 introduction and remains >300 mV positive of E_{cat} after 300 s. Inclusion of 100 µM $Ru(acac)_3$ (**Figure 6A,** green line) for the chloroacetic acid buffer and 100 µM $Me_{10}Fc$ (**Figure 6B**, red line) for the tosylic acid buffer, accelerates the decay of E_{probe}, enabling detection of $E_{cat} = E_{RHE}^{MeCN}$ within ~200 s. These data are in broad agreement with observations in aqueous media and also hold for proton acceptor/donor pairs that are more acidic (A^- = dimethylformamide; $pK_a = 6.1$[45])

or more basic (HA = acetic acid; $pK_a = 23.5$[44]) as shown in Figures S10-S11. As illustrated in **Figure 6C**, the aggregate of these four potential sensing systems covers ~1 V in E_{cat}—a substantial span capable of capturing a wide spectrum of plausibly potential-dependent non-faradaic reactions including hydrogenation, CO_2 reduction, and aerobic oxidation catalysis[46]. In principle, the set of redox sensors summarized in **Figure 6C** can be expanded to include any redox-active molecule as long as it satisfies the three governing criteria detailed above.

Elucidating polarization effects during metal-catalyzed aerobic oxidation reactions

Encouraged by the foregoing findings, we now apply wireless potentiometry to monitor E_{cat} of commercially-available Pt/SiO_2, Pt/Al_2O_3, and Pt/TiO_2 catalysts during aerobic oxidations in aqueous media—a broad reaction class relevant for energy sustainability, decarbonization, and environmental remediation[47,48]. Kinetic analyses of electrode-bound catalysts (e.g., Pt/C) have revealed that metal-catalyzed aerobic oxidations[6,11,20], such as the reaction between O_2 and HCOOH (**Equation 5**), occur via the coupling of countervailing electrochemical half-reactions—for example HCOOH oxidation (**Equation 6**) and O_2 reduction (**Equation 7**).

$$HCOOH + \frac{1}{2}O_2 \rightarrow CO_2 + H_2O \qquad \textbf{Equation 5}$$

$$HCOOH \rightarrow CO_2 + 2H^+ + 2e^- \qquad \textbf{Equation 6}$$

$$\frac{1}{2}O_2 + 2H^+ + 2e^- \rightarrow H_2O \qquad \textbf{Equation 7}$$

Based on these observations we regard aerobic formic acid oxidation catalysis as a model potential-sensitive reaction for which E_{cat} measurement is essential for functional characterization and mechanistic understanding. The role of catalyst polarization during aerobic oxidation of formic acid has, to the best our knowledge, only been studied on carbon-supported metal catalysts because of the precedent necessity of establishing direct electronic contact to macroscopic wires for potential sensing. Wireless potentiometry eliminates this constraint and permits investigation of the role of the oxide support identity (SiO_2, Al_2O_3, TiO_2) on potential-dependent reactivity. As illustrated in **Equation 6**, we measure E_{cat} using 10 μM phosphomolybdate (PMA) as the potential sensor. PMA is analogous to STA and PTA and in acidic media has reversible redox features at ~0.4 V and ~0.65 V vs SHE, enabling potential sensing over the range ~0.2 V to ~0.85 V vs SHE[49–51]. This potential range is well-aligned with previously reported E_{cat} values for aerobic oxidations in aqueous media[6,11,20]. Initial observations evince the viability of the PMA sensor for aerobic formic oxidation. Specifically, the measured transients in rate and potential evolve at comparable timescales, indicating that E_{probe} reflects E_{cat} (Figure S16). Additionally, steady-state measurements of E_{probe} are invariant with sensor concentration ranging from ~5 to ~20 μM PMA, suggesting that presence of PMA does not alter E_{cat} (Figure S17). Finally, steady-state rates of CO_2 formation are identical with or without 10 μM PMA, establishing that these concentration levels are sufficiently dilute to prevent perturbation to catalytic function (Figure S18). In order to facilitate rate-potential correlations, we quantified the turnover frequency, *TOF*, by measuring the rate of CO_2 formation normalized by the number of exposed Pt atoms determined by transmission electron microscopy (Figures S19; Table S1).

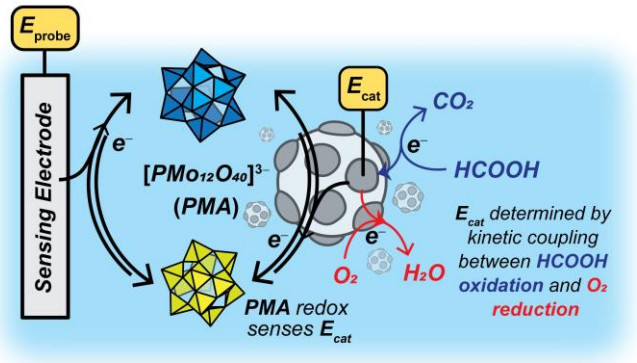

Figure 7 | Wireless potentiometry during aerobic formic acid oxidation. The potential of dispersed Pt/SiO_2 particles (E_{cat}) is determined by the coupling of electrochemical oxidation of HCOOH and reduction of O_2. In turn, E_{cat} specifies the state-of-charge of dilute phosphomolybdate anions (PMA). Outer-sphere electron transfer between PMA and glassy carbon sensing electrode then equilibrates E_{probe} with E_{cat}.

Conventional measurements of rate and reaction order suggest minimal difference in catalysis across the three supports. We measured steady-state *TOF* values as a function of HCOOH concentration (125 – 500 mM) with 1 bar O_2. We find that reaction rates are invariant with stir rate and mass loading, confirming the absence of interparticle transport limitations[52] (Table S2). As shown in **Figure 8A**, CO_2 formation turnover frequencies over Pt catalysts supported on SiO_2 (black squares), Al_2O_3 (red circles), or TiO_2 (blue diamonds) are within ~2× of each other at the same conditions, with nearly identical *TOF* values on Pt/SiO_2 and Pt/TiO_2. The observed rates are also consistent with previously reported measurements using electrode-supported Pt/C catalysts[6]. In addition to similarity in absolute rates, reaction orders in HCOOH, ~½, are also comparable across all oxide-supported catalysts. Together, these conventional measures of catalyst activity suggest that Pt/SiO_2, Pt/Al_2O_3, and Pt/TiO_2 catalyze thermochemical HCOOH oxidation in a similar fashion.

The above apparent commonalities belie underlying differences in catalytic function that are exposed by operando measurement of E_{cat}. **Figure 8B** shows *TOF* and E_{cat} from the same experiments represented in **Figure 8A** with each symbol labeled by the corresponding HCOOH concentration. With each increment in HCOOH concentration, E_{cat} is decreased due to an increase in the rate of e^- donation to Pt via HCOOH oxidation (see **Equation 6**, **Figure 7**). In turn, the decrease in E_{cat} accelerates O_2 reduction until the rates of each half-reaction equalize to furnish the steady-state *TOF* shown in **Figure 8B**. This interplay between e^- donation by HCOOH and e^- scavenging by O_2 is missed by analysis of reaction orders alone but is quantitatively captured by examination of the relationship between *TOF* and E_{cat}. Specifically, the scaling of rate with catalyst potential quantifies the extent to which changes in E_{cat} induced by HCOOH addition serve to accelerate O_2 reduction. **Figure 8B** shows that the rate-potential scaling for O_2 reduction on Pt/TiO_2 (127 mV dec^{-1}) is ~2× steeper than on Pt/SiO_2 and Pt/Al_2O_3 (242 – 289 mV dec^{-1}). These data suggest that, contrary to the findings in **Figure 8A**, Pt/TiO_2 catalysts are functionally distinct from Pt/SiO_2 and Pt/Al_2O_3. These differences are not manifest in HCOOH reaction orders simply because the data in **Figure 8A** and **Figure 8B** sample distinct catalytic phenomena. The reaction order in HCOOH samples the kinetic relevance of *all* steps that consume HCOOH while the O_2 reduction rate-potential scaling samples the kinetic relevance of *electrochemical* steps that consume O_2[53].

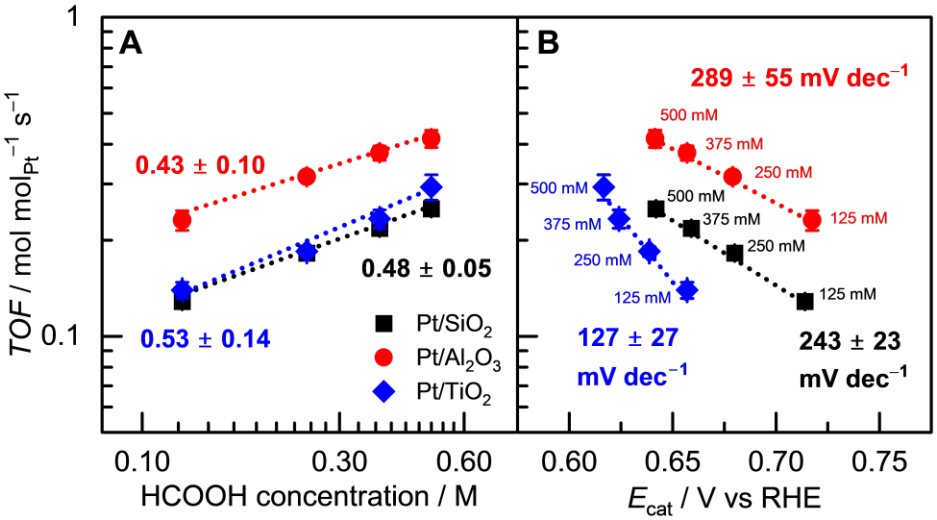

Figure 8 | Aerobic HCOOH oxidation on supported Pt catalysts. Steady-state turnover frequency of CO_2 formation on Pt/SiO_2 (black squares), Pt/Al_2O_3 (red circles), and Pt/TiO_2 (blue diamonds) as a function of **A)** HCOOH concentration and **B)** catalyst potential. Dotted lines are determined by linear fit of corresponding symbols. Slope and standard error in slope of each dotted line are labeled in the corresponding color and quantify **A)** HCOOH reaction order and **B)** rate-potential scaling. Each symbol in **B)** is labeled with the steady-state HCOOH concentration. Conditions: 0.1 M $HClO_4$, 1 bar O_2, ~21 °C, 1 – 5 g/L catalyst, potential measured by GC sensing electrode using 10 μM PMA. See SI for detailed cell design and experimental protocol. Error bars represent standard error of replicate experiments.

Based on data in **Figure 8**, the identity of oxide supports has little effect on the former catalytic phenomena but profoundly influences the latter. We attribute these observations to the following: (1) a constancy in the mechanism of HCOOH activation through fractionally-covered surfaces that give rise to fractional HCOOH reaction order[6,54,55] and (2) differences in the mechanism of O_2 activation resulting from disparate metal site-motif exposure[56], inner sphere reactivity between HCOOH- and O_2-derived intermediates[28], and/or mass transport manifolds within porous supports[11,57]. The observed range of rate-potential scalings (127 – 289 mV dec^{-1}) can be explained by any of these possibilities—each of which has been demonstrated to be consequential during metal-catalyzed aerobic oxidations proceeding through a coupling of electrochemical half-reactions. A systematic investigation of the relevance of these phenomena to HCOOH + O_2 catalysis is

beyond the scope of this work, but the methods and observations herein lay the groundwork to investigate such possibilities through integrated catalyst synthesis, functional catalyst characterization, and detailed kinetic analyses. Moreover, we stress that since catalyst potential is an effective descriptor of a tremendous variety of interfacial polarization phenomena (e.g., electric field-adsorbate dipole interactions, metal-support cooperativity, surface corrosion/passivation), E_{cat} quantification is highly enabling for mechanistic study of *any* potential-sensitive reaction.

CONCLUSION AND OUTLOOK

In this work, we develop a methodology to quantify the open-circuit potential of metal nanoparticles supported on non-conductive oxides—a class of materials used ubiquitously in solid-liquid heterogeneous catalysis. During catalysis, each metal aggregate polarizes to an open-circuit electrochemical potential E_{cat}. This electrochemical process is intimately related to catalytic function at metal-liquid interfaces but has gone largely undetected because of the inability to connect macroscopic wires to microscopic metal nanoparticles supported on electronically insulating oxides. We address this measurement gap by using small concentrations (10 – 100 μM) of electron shuttling agents to establish a solution-phase electrical connection between supported metal catalysts (e.g., Pt/SiO_2) and an *in situ*, catalytically-innocent probe electrode (e.g., glassy carbon). Selection of redox sensors is guided by a simple design heuristic—that the molecular redox potential is within ~180 mV of E_{cat}. As a proof-of-concept demonstration, we use silicotungstate, $[SiW_{12}O_{40}]^{4-/5-/6-}$, to quantify E_{cat} of SiO_2-supported Pt catalysts during H_2/H^+ catalysis in acidic aqueous media. This approach quantifies the equilibrium potential of H_2/H^+, $E_{RHE} = E_{cat}$, within 1 mV both at steady state and throughout catalytic transients initiated by step change in H_2 pressure (0.1 – 1 bar) or pH (1 – 4.46). This *wireless* potential sensing framework is generalizable to *any* reaction medium provided appropriate choice of molecular redox sensor. We demonstrate this principle by detection of $E_{cat} = E_{RHE}$ across 14 orders of magnitude in H^+ activity in water and acetonitrile solvents using organic molecules and inorganic coordination complexes as electron shuttles depending on solvent identity and pH. From the learnings established in these validation studies, we measure E_{cat} during aerobic oxidation of formic acid catalyzed by Pt supported on SiO_2, Al_2O_3, and TiO_2—three of the most commonly used catalyst supports. Simultaneous quantification of turnover frequency, *TOF*, and E_{cat} reveals rate-potential scalings that vary by 2.3× (127 – 289 mV dec^{-1}) amongst the three studied catalyst formulations. These differences in catalytic function are not quantifiable by conventional thermochemical analyses and exemplify the importance of measuring E_{cat} during metal-catalyzed thermochemical reactions even if the support material is non-conductive. Given that E_{cat} reports on a wealth of catalytic information (e.g., adsorbate coverage, surface reconstruction, interfacial electric field) the methodology developed here opens the door to a rich array of mechanistic insights and design principles that utilize this previously inaccessible parameter.

Data availability

The data that support the findings of this study are included in the published article (and its Supplementary Information) or available from the corresponding author on reasonable request.

Corresponding Author

*yogi@mit.edu

Acknowledgement

The authors thank the entire Surendranath Lab for their support and scientific discussions. This work was supported by the Gordon and Betty Moore Foundation (Grant ID: GBMF11510). N.K.R. thanks the generous support from the Arnold O. Beckman Postdoctoral Fellowship.

Author Contributions

N.K.R. and Y.S. conceived the research and developed experiments. N.K.R. conducted the majority of the experiments. K.S.W. conducted characterization experiments and contributed to data analysis. N.K.R. and Y.S wrote the manuscript with input from all authors.

Competing Interests

The authors declare no competing financial interest.

References

1. Shangguan, J. & Chin, Y.-H. C. Kinetic Significance of Proton−Electron Transfer during Condensed Phase Reduction of Carbonyls on Transition Metal Clusters. *ACS Catal.* **9**, 1763–1778 (2019).

2. Zhao, Z. *et al.* Solvent-mediated charge separation drives alternative hydrogenation path of furanics in liquid water. *Nat. Catal.* **2**, 431–436 (2019).

3. Zope, B. N., Hibbitts, D. D., Neurock, M. & Davis, R. J. Reactivity of the Gold/Water Interface During Selective Oxidation Catalysis. *Science (80-.).* **330**, 74–78 (2010).

4. Cheng, G. *et al.* Importance of interface open circuit potential on aqueous hydrogenolytic reduction of benzyl alcohol over Pd/C. *Nat. Commun.* **13**, (2022).

5. Wesley, T. S., Román-Leshkov, Y. & Surendranath, Y. Spontaneous Electric Fields Play a Key Role in Thermochemical Catalysis at Metal-Liquid Interfaces. *ACS Cent. Sci.* **7**, 1045–1055 (2021).

6. Ryu, J. *et al.* Thermochemical aerobic oxidation catalysis in water can be analysed as two coupled electrochemical half-reactions. *Nat. Catal.* **4**, 742–752 (2021).

7. Mallat, T. & Baiker, A. Catalyst potential measurement: A valuable tool for understanding and controlling liquid phase redox reactions. *Top. Catal.* **8**, 115–124 (1999).

8. Adams, J. S., Kromer, M. L., Rodríguez-López, J. & Flaherty, D. W. Unifying Concepts in Electro- And Thermocatalysis toward Hydrogen Peroxide Production. *J. Am. Chem. Soc.* **143**, 7940–7957 (2021).

9. Bockris, J. O., Reddy, A. & Gamboa-Aldeco, M. *Modern Electrochemistry 2A: Fundamentals of Electrodics*. (Springer, 2000).

10. Tao, Q. *et al.* Interaction of C_1 Molecules with a Pt Electrode at Open Circuit Potential: A Combined Infrared and Mass Spectroscopic Study. *J. Phys. Chem. C* **118**, 6799–6808 (2014).

11. DiCosimo, R. & Whitesides, G. M. Oxidation of 2-propanol to acetone by dioxygen on a platinized electrode under open-circuit conditions. *J. Phys. Chem.* **93**, 768–775 (1989).

12. Tokarev, A. V *et al.* Kinetic behaviour of electrochemical potential in three-phase heterogeneous catalytic oxidation reactions. *J. Mol. Catal. A Chem.* **255**, 199–208 (2006).

13. Qi, X. *et al.* Potential–Rate Correlations of Supported Palladium-Based Catalysts for Aqueous Formic Acid Dehydrogenation. *J. Am. Chem. Soc.* **146**, 9191–9204 (2024).

14. Mallat, T. & Baiker, A. Oxidation of alcohols with molecular oxygen on platinum metal catalysts in aqueous solutions. *Catal. Today* **19**, 247–283 (1994).

15. Sauvé, E. R. *et al.* Open circuit potential decay transients quantify interfacial pH swings during high current density hydrogen electrocatalysis. *Joule* **8**, 728–745 (2024).

16. Vayenas, C. G. Bridging electrochemistry and heterogeneous catalysis. *J. Solid State Electrochem.* **15**, 1425–1435 (2011).

17. Lodaya, K. M. *et al.* An electrochemical approach for designing thermochemical bimetallic nitrate hydrogenation catalysts. *Nat. Catal.* **7**, 262–272 (2024).

18. Daniel, I. T. *et al.* Electrochemical Polarization of Disparate Catalytic Sites Drives Thermochemical Rate Enhancement. *ACS Catal.* **13**, 14189–14198 (2023).

19. van der Plas, J. F. & Barendrecht, E. Electrocatalytic hydrogenation processes at controlled potential—3. Measurement of the catalyst potential. *Electrochim. Acta* **25**, 1477–1480 (1980).

20. Howland, W. C., Gerken, J. B., Stahl, S. S. & Surendranath, Y. Thermal Hydroquinone Oxidation on Co/N-doped Carbon Proceeds by a Band-Mediated Electrochemical Mechanism. *J. Am. Chem. Soc.* **144**, 11253–11262 (2022).

21. An, H., Sun, G., Hülsey, M. J., Sautet, P. & Yan, N. Demonstrating the Electron–Proton-Transfer Mechanism of Aqueous Phase 4-Nitrophenol Hydrogenation Using Unbiased Electrochemical Cells. *ACS Catal.* **12**, 15021–15027 (2022).

22. Anson, C. W. & Stahl, S. S. Mediated Fuel Cells: Soluble Redox Mediators and Their Applications to Electrochemical Reduction of O2 and Oxidation of H2, Alcohols, Biomass, and Complex Fuels. *Chem. Rev.* **120**, 3749–3786 (2020).

23. Stergiou, A. D. & Symes, M. D. Organic transformations using electro-generated polyoxometalate redox mediators. *Catal. Today* **384–386**, 146–155 (2022).

24. Adams, J. S. *et al.* Solvent molecules form surface redox mediators in situ and cocatalyze O2 reduction on Pd. *Science (80-.).* **371**, 626–632 (2021).

25. Kummer, J. T. & Oei, D. G. A chemically regenerative redox fuel cell. *J. Appl. Electrochem.* **12**, 87–100 (1982).

26. Westendorff, K. S., Hülsey, M. J., Wesley, T. S., Román-Leshkov, Y. & Surendranath, Y. Electrically driven proton transfer promotes Brønsted acid catalysis by orders of magnitude. *Science (80-.).* **383**, 757–763 (2024).

27. Hoque, M. A., Gerken, J. B. & Stahl, S. S. Synthetic dioxygenase reactivity by pairing electrochemical oxygen reduction and water oxidation. *Science (80-.).* **383**, 173–178 (2024).

28. Bates, J. S. *et al.* Chemical and Electrochemical O2 Reduction on Earth-Abundant M-N-C Catalysts and Implications for Mediated Electrolysis. *J. Am. Chem. Soc.* **144**, 922–927 (2022).

29. Sun, Y., Dai, Y., Liu, Y. & Chen, S. A rotating disk electrode study of the particle size effects of Pt for the hydrogen oxidation reaction. *Phys. Chem. Chem. Phys.* **14**, 2278–2285 (2012).

30. Durst, J., Simon, C., Hasché, F. & Gasteiger, H. A. Hydrogen Oxidation and Evolution Reaction Kinetics on Carbon Supported Pt, Ir, Rh, and Pd Electrocatalysts in Acidic Media. *J. Electrochem. Soc.* **162**, F190 (2015).

31. Roberts, J. A. S. & Bullock, R. M. Direct Determination of Equilibrium Potentials for Hydrogen Oxidation/Production by Open Circuit Potential Measurements in Acetonitrile. *Inorg. Chem.* **52**, 3823–3835 (2013).

32. Pope, M. T. & Varga, G. M. J. Heteropoly Blues. I. Reduction Stoichiometries and Reduction Potentials of Some 12-Tungstates. *Inorg. Chem.* **5**, 1249–1254 (1966).

33. Mallat, T., Bodnar, Z. & Baiker, A. Partial oxidation of water-insoluble alcohols over Bi-promoted Pt on alumina. Electrochemical characterization of the catalyst in its working state. *Stud. Surf. Sci. Catal.* **78**, 377–384 (1993).

34. Conway, B. E. & Tilak, B. V. Behavior and Characterization of Kinetically Involved Chemisorbed Intermediates in Electrocatalysis of Gas Evolution Reactions. in (eds. Eley, D. D., Pines, H. & Weisz, P. B. B. T.-A. in C.) vol. 38 1–147 (Academic Press, 1992).

35. Batista, B. C. & Varela, H. Open Circuit Interaction of Formic Acid with Oxidized Pt Surfaces: Experiments, Modeling, and Simulations. *J. Phys. Chem. C* **114**, 18494–18500 (2010).

36. Fish, M. J. & Ollis, D. F. Characterization of enantioselective hydrogenation catalysts: Transient electrochemical oxidation of d-(+)-tartaric acid on nickel. *J. Catal.* **50**, 353–363 (1977).

37. Jürgensen, A. & Moffat, J. B. The stability of 12-molybdosilicic, 12-tungstosilicic, 12-molybdophosphoric and 12-tungstophosphoric acids in aqueous solution at various pH. *Catal. Letters* **34**, 237–244 (1995).

38. Michaelis, L. & Hill, E. S. The viologen indicators. *J. Gen. Physiol.* **16**, 859–873 (1933).

39. Ito, M. & Kuwana, T. Spectroelectrochemical study of indirect reduction of triphosphopyridine nucleotide. I. Methyl viologen, ferredoxin-TPN-reductase and TPN. *J. Electroanal. Chem.* **32**, 415–425 (1971).

40. Bird, C. L. & Kuhn, A. T. Electrochemistry of the viologens. *Chem. Soc. Rev.* **10**, 49–82 (1981).

41. Venturi, M., Mulazzani, Q. G. & Hoffman, M. Z. Radiolytically-induced one-electron reduction of methyl

viologen in aqueous solution: Stability of the radical cation in acidic and highly alkaline media. *Radiat. Phys. Chem.* **23**, 229–236 (1984).

42. Datta, M., Jansson, R. E. & Freeman, J. J. In Situ Resonance Raman Spectroscopic Characterization of Electrogenerated Methyl Viologen Radical Cation on Carbon Electrode. *Appl. Spectrosc.* **40**, 251–258 (1986).

43. Michaelis, L. Occurrence and Significance of Semiquinone Radicals. *Ann. N. Y. Acad. Sci.* **40**, 39–76 (1940).

44. Kütt, A. *et al.* Strengths of Acids in Acetonitrile. *European J. Org. Chem.* **2021**, 1407–1419 (2021).

45. Izutsu, K. *Acid-Base Dissociation Constants in Dipolar Aprotic Solvents*. (Blackwell: Oxford, 1990).

46. Pegis, M. L. *et al.* Standard Reduction Potentials for Oxygen and Carbon Dioxide Couples in Acetonitrile and N,N-Dimethylformamide. *Inorg. Chem.* **54**, 11883–11888 (2015).

47. Chheda, J. N., Huber, G. W. & Dumesic, J. A. Liquid-phase catalytic processing of biomass-derived oxygenated hydrocarbons to fuels and chemicals. *Angew. Chemie - Int. Ed.* **46**, 7164–7183 (2007).

48. Guo, Z. *et al.* Recent advances in heterogeneous selective oxidation catalysis for sustainable chemistry. *Chem. Soc. Rev.* **43**, 3480–3524 (2014).

49. Freund, M. S. & Lewis, N. S. Irreversible Electrocatalyic Reduction of V(V) to V(IV) Using Phosphomolybdic Acid. *Inorg. Chem.* **33**, 1638–1643 (1994).

50. Oh, H. *et al.* Phosphomolybdic acid as a catalyst for oxidative valorization of biomass and its application as an alternative electron source. *ACS Catal.* **10**, 2060–2068 (2020).

51. Tanaka, N., Unoura, K. & Itabashi, E. Voltammetric and spectroelectrochemical studies of dodecamolybdophosphoric acid in aqueous and water-dioxane solutions at a gold-minigrid optically transparent thin-layer electrode. *Inorg. Chem.* **21**, 1662–1666 (1982).

52. Flaherty, D. W. & Bhan, A. Improving the rigor and reproducibility of catalyst testing and evaluation in the laboratory. *J. Catal.* **431**, 115408 (2024).

53. Baz, A. & Holewinski, A. Predicting macro-kinetic observables in electrocatalysis using the generalized degree of rate control. *J. Catal.* **397**, 233–244 (2021).

54. Lović, J. D. *et al.* Kinetic study of formic acid oxidation on carbon-supported platinum electrocatalyst. *J. Electroanal. Chem.* **581**, 294–302 (2005).

55. Kwon, S., Lin, T. C. & Iglesia, E. Elementary steps and site requirements in formic acid dehydration reactions on anatase and rutile TiO2 surfaces. *J. Catal.* **383**, 60–76 (2020).

56. Adams, J. S. *et al.* Distinct Site Motifs Activate O_2 and H_2 on Supported Au Nanoparticles in Liquid Water. *ACS Catal.* **14**, 3248–3265 (2024).

57. Nicoletti, J. W. & Whitesides, G. M. Liquid-phase oxidation of 2-propanol to acetone by dioxygen using supported platinum catalysts. *J. Phys. Chem.* **93**, 759–767 (1989).